ELSEVIER

Contents lists available at ScienceDirect

Agricultural Water Management

journal homepage: www.elsevier.com/locate/agwat





Measurement and estimation of evapotranspiration in a maize field: A new method based on an analytical water flux model

Yutong Liu^a, Yili Lu^{a,b,*}, Morteza Sadeghi^c, Robert Horton^d, Tusheng Ren^a

- ^a College of Land Science and Technology, China Agricultural University, Beijing 100193, China
- ^b State Key Laboratory of Efficient Utilization of Agricultural Water Resources, Beijing 100083, China
- ^c California Department of Water Resources, Sacramento, CA 95814, USA
- ^d Agronomy Department, Iowa State University, Ames, IA 50011, USA

ARTICLE INFO

Handling Editor - Dr Z Xiying

Keywords: Evapotranspiration Soil water flux Soil water content Richards' equation

ABSTRACT

Quantifying evapotranspiration (ET) in rainfed cropping systems can be challenging due to complicated interactions among site-specific soil, plant, and management factors. In Northeast China, ET and soil water status in maize fields often display strong spatial and temporal variations due to the changes in tillage practice, planting pattern, and maize plant density. Previous studies have shown that near-surface soil water content (θ) observations at multiple scales provide the potential to estimate surface soil water fluxes. In this study, we introduced a new method to estimate daily field ET by using a soil water flux model mainly based on the time-series of θ at a depth of 2.5 cm. The new method required a calibration of soil water diffusivity with maximum net water flux in the near-surface soil layer, which was related to precipitation redistribution below the canopy. Finally, the new method was evaluated using observed ET values over a 2-year period in a maize field, where independent measurements of soil water evaporation (E) and transpiration (T) were made with heat-pulse sensors and sapflow gauges, respectively. Field observations showed that E dominated water loss during the seedling stage (16% of total ET). As the canopy was fully developed, E sharply decreased to a value of 0.4 mm d⁻¹, and T accounted for about 89% of ET since the silking stage. The new method to estimate ET performed well in drying periods, while it tended to underestimate ET in wet periods with substantial infiltration into the surface layer. On rain-free days, the ET values estimated with the new method matched well with the measured E+T values, with R^2 and RMSE values of 0.85 and 1.93 mm d^{-1} . Therefore, the new approach provides an effective way to quantify maize ET.

1. Introduction

Accurate determination of evapotranspiration (*ET*) in farmlands remains a challenge due to the many influencing factors in the soil-plant-atmosphere system, e.g., climate condition, soil type, tillage practice, and planting pattern (Allen et al., 1998). *ET* is a highly dynamic variable, especially in agricultural systems with various cropping patterns. For example, in Northeast China where the paired-row planting system is widely used, the large row spacing difference between the plant rows and the pairs of rows leads to nonuniform surface soil conditions and canopy cover at the field scale during maize growing season (*Sharratt*, 1993; He et al., 2010). In a rainfed field with alternating row spacings, it remains a challenge to quantify *ET* due to the complexities in both measurements and modeling of *ET* variations across the fields.

Several techniques have been developed to measure ET. Weighing lysimeters determine in-situ ET by direct measurements of the change in mass over time, but lysimeters are expensive and not commonly available (Rana and Katerji, 2000). The soil water balance method can be used to estimate ET rates by monitoring changes in root-zone water status with multiple in-situ soil water content (θ) observations at the point scale (Holmes, 1984). Special attention is needed because errors in estimating ET are likely to occur immediately following wetting events due to the formation of deep percolation (Liu et al., 2006; Cholpankulov et al., 2008). Micrometeorological methods, such as the eddy covariance and Bowen ratio methods, have been widely applied to estimate ET rates. However, these approaches require stable atmospheric conditions and a relatively uniform underlying surface to satisfy the methodological principles (Fuchs and Tanner, 1970; Baldocchi et al., 2001).

^{*} Corresponding author at: College of Land Science and Technology, China Agricultural University, Beijing 100193, China. *E-mail address:* huyili@cau.edu.cn (Y. Lu).

Recently, canopy chamber methods were used to determine ET with the approach of enclosing air at the plant canopy level using a control volume to monitor vapor concentration changes over time (Luo et al., 2018). In this method, the canopy chambers have to be opened and closed between consecutive measurements to avoid chamber-induced canopy microclimate changes (Wang et al., 2018). Recently, the combined approach that determines soil water evaporation (E) with the soil-placed heat-pulse sensors and monitors plant transpiration (T) with sap-flow techniques, has been applied to quantify the actual ET and to partition ET into E and T at the same time (Xiao et al., 2016; Wang et al., 2021). The combined method can capture variations in ET under field conditions with fine spatial-temporal resolutions.

Physical- and empirical-based ET models have drawn attention for a long time. A classical analytical model, known as the Penman-Monteith (PM) equation, was established based on one-dimensional aerodynamic processes and energy balance theory (Penman, 1948; Monteith, 1965). Application of the PM equation can be challenging due to the requirements for accurate information on several variables including meteorological conditions and aerial boundary layer resistances (Evett et al., 2012). To improve the transferability of the PM model across regions with different climates and crops, the FAO introduced the single and dual crop coefficient methods to estimate the actual evapotranspiration for a specific cropland (Allen et al., 1998). The actual evapotranspiration is obtained by multiplying evapotranspiration with the crop coefficients (K_c) that require adjustment or calibration depending on the crop types, climate conditions, and irrigation patterns (Allen et al., 2011; Pereira et al., 2015).

Over the last few decades, the application of remote sensing techniques has provided estimations of ET over large areas based on surface energy balance theory and ancillary data (i.e., surface roughness and leaf area index) (Schmugge et al., 2002; Lu et al., 2016). However, the relatively coarse resolution of ET data may cause problems when downscaling them to make daily field estimations due to the variabilities of soil texture, plant species, and meteorological conditions (Cammalleri et al., 2013). Recently, the availability of surface θ observations from large monitoring networks (e.g., SCAN, COSMOS, and CRN) using proximal or remote sensing techniques have enabled estimates of the hydrologic status of near-surface soil layer across multiple scales (Zreda et al., 2008; Coopersmith et al., 2015). As a state variable of the near-surface soil layer, θ values in vegetated systems are not only affected by atmospheric conditions but also closely related to soil properties and plant water use (Akbar et al., 2018). Numerous studies have used the Richards' equation with known boundary and initial conditions to interpret precipitation, ET, runoff, and net outcomes for all of the water balance components to explore the relationship between soil surface θ and surface fluxes (Black et al., 1969; Koster et al., 2018; Purdy et al., 2018; Wang et al., 2020). Sadeghi et al. (2019), (2022) introduced an inverse and an approximate solution to the Richards' equation to calculate the net soil water flux at the near-surface soil layer. For maize fields with large crop water use and significant temporal θ fluctuations in the growing season, previous endeavors to estimate surface soil water flux provide an effective way to quantify the field ET.

In this study, a new method is presented to estimate ET in a maize field in Northeast China with near-surface θ dynamics using a surface soil water flux model. Field E and T rates, which were measured independently using heat-pulse and sap flow sensors, were applied for quantifying the temporal patterns of field ET in a paired-row planting system, and for evaluating the performance of the new method.

2. Theory

We developed a new method to estimate daily ET rates based on the soil water balance theory and the soil water flux model of Sadeghi et al. (2019). Assuming that daily soil water fluxes are one-dimensional, the net water flux for the near-surface layer (f) of a bare soil can be defined as follows,

$$f = ET - I = ET - (P - R) \tag{1}$$

where f is positive for upward flow and negative for downward flow, I is soil water infiltration rate, P is daily precipitation amount, and R is the rate of surface runoff.

In a level crop field where R can be ignored, the rainwater that reaches the soil surface is less than P due to canopy interception (I_c) , so f can be expressed as,

$$f = ET - (P - I_c) \tag{2}$$

During a drying period, the term I in Eq. (1) vanishes, and the absolute value of f is an estimate of ET,

$$f = ET, \ f > 0 \tag{3}$$

Sadeghi et al. (2019) presented a model to estimate f using the time series of near-surface θ values. The model was derived from an analytical solution to the linearized Richards' equation proposed by Warrick (1975). By inverting the Warrick (1975) solution, the following equation is obtained,

$$F_{N} = \begin{cases} \frac{\Theta_{N}(Z)e^{0.5Z - 0.25M}}{U(Z,\Delta M)}[N=1] \\ F_{1} + \frac{\Theta_{N}(Z)e^{0.5Z - 0.25M} - F_{1}U(Z,M)}{U(Z,\Delta M)}[N=2] \\ F_{N-1} + \frac{1}{U(Z,\Delta M)} \begin{cases} \Theta_{N}(Z)e^{0.5Z - 0.25M} - F_{1}U(Z,M) \\ -\sum_{i=3}^{N} (F_{i-1} - F_{i-2})U(Z,[N-i+2]\Delta M) \end{cases} [N > 2] \end{cases}$$

$$(4)$$

where subscripts i to N denote the time steps with a ΔM interval. Note that downward flux is set as positive in the original model. The M, Z, Θ , and F are dimensionless representations of time t, soil depth z, θ , and f, which are defined as,

$$\begin{cases}
M = \frac{k^2 t}{D} \\
Z = \frac{kz}{D} \\
\Theta = \left(\frac{\theta - \theta_{\infty}}{\theta_{\infty}}\right) e^{-0.5Z + 0.25M} \\
F = \frac{f - k\theta_{\infty}}{k\theta_{\infty}}
\end{cases}$$
(5)

According to the linearized Richards' equation, D is simplified as the constant soil water diffusivity, and k is simplified as the constant slope of the soil hydraulic conductivity- θ function in Eqs. (4) and (5). The θ_{∞} denotes soil water content at the bottom boundary, and the function U in Eq. (4) is given as (Sadeghi et al., 2019),

$$U(Z,M) = -0.5e^{Z}(Z+M+1)\operatorname{erfc}\left[0.5\left(\frac{Z}{\sqrt{M}}+\sqrt{M}\right)\right] + \sqrt{\frac{M}{\pi}}e^{-\left[0.5\left(\frac{Z}{\sqrt{M}}-\sqrt{M}\right)\right]^{2}} + 0.5\operatorname{erfc}\left[0.5\left(\frac{Z}{\sqrt{M}}-\sqrt{M}\right)\right]$$
(6)

Based on Sadeghi et al. (2019), a sensitivity analysis showed that modeled f values were insensitive to k values between 0.0001 and 1 cm d^{-1} , so that k could be set as an arbitrary value (e.g., 0.01 cm d^{-1}) in practice. In contrast, the modeled f values were quite sensitive to values of D, indicating a requirement of D calibration.

Following Sadeghi et al. (2019), for very small Z and M values, U(M) in Eq. (6) can be approximately reduced to,

$$U \approx \sqrt{M} \tag{7}$$

Based on Eqs. (5) and (7), Sadeghi et al. (2019) derived the following empirical equation to calibrate *D* values,

$$D = D' \left(\frac{f_{\text{max}}}{f'_{\text{max}}}\right)^2 \tag{8}$$

where D' is set as an arbitrary value for D (e.g., $100 \text{ cm}^2 \text{ d}^{-1}$), f_{max} and f_{max} are the initial and actual maximum net soil water fluxes for near-surface soil layer.

In the new method, the observed time-series of θ data and site-specific D values are required as inputs to Eqs. (4)-(6) to determine f. Under field conditions, local D needs to be determined specifically from the values of f'_{\max} and f_{\max} with Eq. (8). In this study, for the purpose of accounting for the dynamic changes of D caused by θ variation in response to repeated wetting and drying cycles, we propose to calibrate D using the following procedures.

Firstly, to account for the seasonal variations of D in the maize field, we divided the observation period into several sub-periods based on the magnitude of rainfall events, i.e., a large precipitation event (P > 30 mm d⁻¹) indicates an obvious change of θ in the near-surface soil layer. Therefore, the observation period was divided into (n+1) subperiods based on the number (n) of large precipitation events.

Secondly, in each sub-period, we used θ data and D' as inputs in Eqs. (4)-(6) to obtain the initial f values, in which the maximum f value (f'_{max}) and the corresponding day (calibration day) could be identified.

Thirdly, in each sub-period, we determined $f_{\rm max}$ on the calibration day. The $f_{\rm max}$ occurrence was usually accompanied by a large P event, during which small ET values could be ignored, so that Eq. (2) became,

$$f_{\text{max}} = (P - I_c)_{\text{max}} \tag{9}$$

To determine I_c in a rainfed maize field, we adopted the equation proposed by Zhang et al. (2023), where they estimated I_c from P, precipitation duration (D_u), and the leaf area index (LAI),

$$I_c = -0.0675 \times D_u + 0.1271 \times LAI \times P \tag{10}$$

From Eqs. (9) and (10), the f_{max} value could be obtained,

$$f_{\text{max}} = P - (-0.0675 \times D_u + 0.1271 \times LAI \times P)$$
 (11)

Finally, we used f_{max} , D', and f_{max} as inputs in Eq. (8) to determine the specific D values in each sub-period. The updated D values were then used to obtain the modeled f values by using Eqs. (4)-(6).

In summary, the f values in a rainfed maize field can be calculated based on the calibrated D by following the previously stated procedures (1)-(4) with known daily θ , P, D_{u} , and LAI during the observation period. Then ET is determined from f (Eq. (3)). In this study, the calculated D, f_{\max} , and f_{\max} values are listed in Table A1 of Appendix A.

3. Materials and methods

3.1. Experimental field

A 2-year field experiment was performed at the Lishu Experiment Station of China Agricultural University ($43^{\circ}16'N$, $124^{\circ}26'E$) in 2020 and 2021. The site is located in Northeast China with a humid continental monsoon climate. The long-term annual average temperature is 5.9°C, and the annual average precipitation is 556 mm. The soil is a typical Mollisol with a clay loam texture (24% sand and 31% clay, USDA soil classification system). Maize ($Zea\ mays\ L$.) was planted in a paired-row planting pattern, with a spacing of 40 cm between two plant rows and 100 cm between two pairs of the rows. The spacing between two adjacent plants in a row was about 20 cm. The rows were east-west orientated. Table 1 shows the dates of maize growing stages in the 2020 and 2021 seasons.

Table 1
Maize growing stages in 2021 and 2022 crop seasons.

Year	Maize growing stages						
2020 2021	Seedling 5/10–6/22 5/15–6/30	Jointing 6/23–7/29 7/1–8/8	Silking 7/30–9/2 8/9–9/11	Maturing 9/3–10/10 9/12–10/15			

3.2. Field measurements

Soil and crop parameters, including θ , E, T, and LAI, were measured during the maize growing seasons in 2020 and 2021. A TDR100 system (Campbell Scientific Inc., Logan, UT) was used to monitor θ at a depth of 2.5 cm from May 15 to September 20 in 2020, and from May 25 to October 15 in 2021. The TDR sensors (70-mm needle length, 2-mm needle diameter, and 20-mm needle-to-needle spacing) were placed at the positions between two pairs of the rows, located at distances of 15 cm and 50 cm from the plant row. TDR- θ values were measured every hour and averaged to produce the daily θ values. After sensor installation, new maize plants were transplanted in the measurement area. To ensure a good crop stand, the maize seedlings were irrigated with 100 mL plant⁻¹ water each day from June 2–7 in 2020, but no additional irrigation was provided during the observation period.

Leaf area was measured once a week with a ruler on 6 representative plants to obtain LAI from July 6 to September 20 in 2020, and from June 12 to September 28 in 2021. A nearby weather station monitored the air temperature (T_a) , relative humidity (RH), wind speed (WS), solar radiation (R_s) , and precipitation (P) every 30 minutes. The θ , as well as LAI, P, and D_u data were used to estimate ET values following the calibration procedures (1)-(4) and Eq. (3). Finally, we estimated ET values from daily TDR- θ data collected at the two locations and used the mean value of the two locations to represent the daily estimated ET value in the maize field.

To validate the performance of the new method, heat pulse sensors and sap flow gauges were used to make independent measurements of E and T. To measure E, multi-needle heat-pulse probes, which were installed near the TDR sensors, were controlled with a CR3000 data logger (Campbell Scientific Inc., Logan, UT). Temperature rises after each heat pulse were determined once an hour, so that soil heat capacity (C) and thermal conductivity (λ) were derived by using a nonlinear regression technique (Zhang et al., 2014). With known soil temperature (T_s) and soil thermal properties (C, λ) , the soil temperature gradients $(\Delta T_s/\Delta z)$, sensible heat fluxes (G), changes of soil sensible heat storage (ΔS) , and E rates at different depths were determined (Heitman et al., 2008).

Soil heat flux G was calculated with Fourier's law,

$$G = -\lambda \frac{\Delta T_s}{\Delta z} \tag{12}$$

Changes in sensible heat storage ΔS in a soil layer were calculated by using the calorimetric method (Ochsner et al., 2007),

$$\Delta S = \sum_{i=1}^{N} C_{i,j-1} \frac{T_{s,i,j} - T_{s,i,j-1}}{t_{i,j} - t_{i,j-1}} (z_i - z_{i-1})$$
(13)

Hourly E was obtained from the sensible heat balance (SHB) equation,

$$(G_1 - G_2) - \Delta S = LE \tag{14}$$

where G_1 and G_2 were the sensible heat fluxes at the top and bottom boundary for a specific soil layer, and L was the latent heat of vaporization (Forsythe, 1964).

$$L = 2.49463 \times 10^9 - 2.247 \times 10^6 T_s \tag{15}$$

When the soil surface was undergoing stage-1 evaporation after rainfall events, we applied the modified sensible heat balance theory to estimate water evaporation from the soil surface (Xiao et al., 2014),

$$(R_n - G_2) - \Delta S = LE \tag{16}$$

where R_n (W m⁻²) was the net radiation fluxes measured at 1-hour intervals with a net radiometer positioned 10 cm above the soil surface. Xiao et al. (2014) suggested using Eq. (16) when θ was greater than 0.25 m³ m⁻³ and otherwise using Eq. (14) based on the clay loam soil texture and the structure, in which the critical value was determined by the inflection point of the soil water retention curve. The hourly *E* values were calculated and summed up into daily values. Finally, the daily *E* values at the two locations between the two pairs of the rows were averaged to obtain a single value of under-canopy *E* in the maize field.

Plant transpiration rate was monitored with the sap-flow method from June 30 to September 20 of 2020 and from July 11 to October 15 of 2021. The sap flow gauges (Flow32-1 K system, Dynamax, Houston, TX, USA) were installed on maize stems at a height of about 20 cm above the ground surface. The sap flow velocity of maize was recorded at a 30-min interval with a CR1000 datalogger (Campbell Scientific Inc., Logan, UT). To avoid heat injury to the plants, we shifted the target maize plants every 7 days. The gauges were also shifted to new plants immediately after rainfall events to avoid any errors caused by rainwater. For maize plants at different growing stages, variable-sized gauges (ranging from SGB13 to SGB25) were selected to ensure a close contact between the gauges and maize stems with the development of maize. Finally, sap flow velocity (g h⁻¹) was adjusted following the Wang et al. (2017) calibration equation and converted into daily $T \text{ (mm d}^{-1})$ by multiplying with the plant density N_p/A (plants m⁻²), where N_n is the number of plants in the field and A is field area (m^2).

4. Results and discussion

4.1. Meteorological conditions

The dynamics of near-surface θ in the row-cropped fields are determined interactively by meteorological conditions (e.g., P and RH), soil water processes (e.g., I and E), and crop factors (e.g., root water uptake and canopy development) (Famiglietti et al., 1999; Metzger et al., 2017). Fig. 1 shows the climatic conditions during the observation periods in 2020 (128 days) and 2021 (144 days). Strong temporal R_S variations

occurred in both years, ranging from 1.6 to 31.4 MJ m $^{-2}$ d $^{-1}$ in 2020 and from 1.1 to 31.3 MJ m $^{-2}$ d $^{-1}$ in 2021, with the highest and lowest values in the jointing and the maturing stage, respectively. The daily T_a showed seasonal patterns ranging from 11.5°C (May 20) to 28.5°C (June 8) in 2020 and 6.2°C (October 15) to 27.8°C (July 27) in 2021. The maximum value of WS was 5.4 m s $^{-1}$ in 2020 and 4.8 m s $^{-1}$ in 2021. The RH values stayed low during the seedling stages with average daily values of 68% (2020) and 73% (2021), and increased thereafter to values of 79% from jointing to maturing stages for the two growing seasons, which correlated negatively with WS.

The high WS and low RH during the seedling stages induced a relatively large vapor pressure deficit, which resulted in significant water vapor exchanges between the soil and atmosphere. Meanwhile, the high R_s and T_a values during the seedling and jointing stages indicated that there was sufficient energy available for E and T during this period.

4.2. Precipitation, soil water content, and crop growth

Fig. 2 shows the P, LAI, TDR-measured θ dynamics, and the net P calculated from Eq. (11). During the two maize growing seasons, the total amount of precipitation was 581 mm in 2020 and 568 mm in 2021. Precipitation events were distributed unevenly during both crop growing seasons. In 2020, a large amount of rainfall occurred in the silking (227 mm) and maturing stages (163 mm) compared to those in the seedling (93 mm) and jointing stages (98 mm). In 2021, rainfalls were distributed more evenly, with slightly larger amounts during the seedling (153 mm) and jointing (165 mm) stages and relatively smaller amounts during the silking (137 mm) and maturing (113 mm) stages.

In both years, with the development of maize canopies, LAI increased slowly during the seedling stage (0–0.9), increased rapidly during the jointing stages to values around 4.5, reached the maximum (> 4.6) in the silking stages (full canopy cover), and decreased gradually thereafter. Dynamic changes in LAI led to rainwater redistribution below the crop canopy, as indicated by the dynamics of net P during the growing season (Hupet and Vanclooster, 2005; Metzger et al., 2017). Fig. 2c shows the net P calculated from Eq. (11). During the seedling stage, the net P below the canopy equaled P, indicating no I_C due to the small maize plant size. As LAI increased rapidly during the jointing stage, the net P accounted for 73% of the P on average. After the full-cover status was

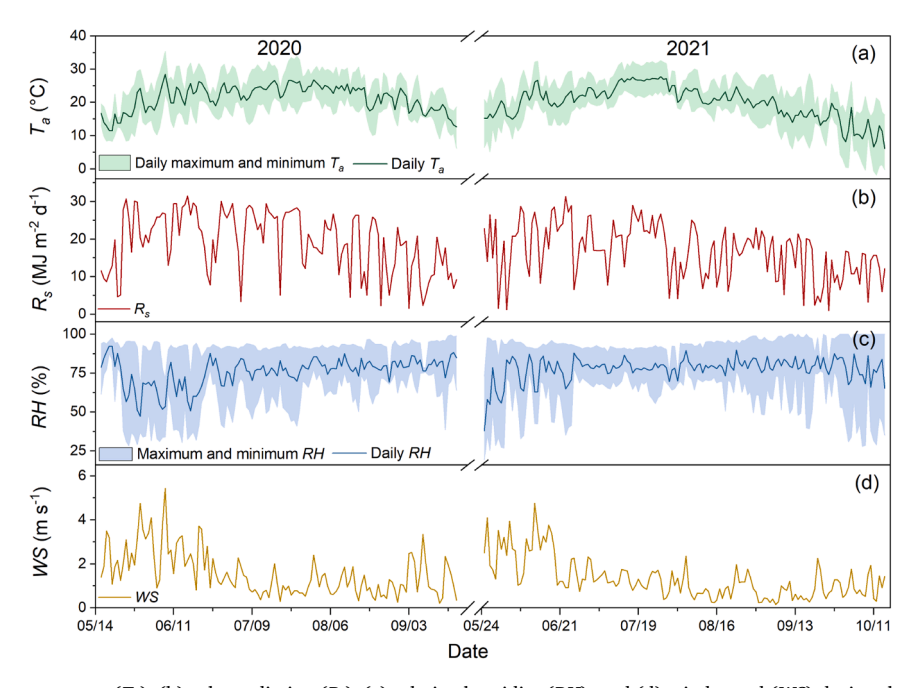


Fig. 1. Dynamics of (a) air temperature (T_a), (b) solar radiation (R_s), (c) relative humidity (RH), and (d) wind speed (WS) during the observation periods of 2020 and 2021.

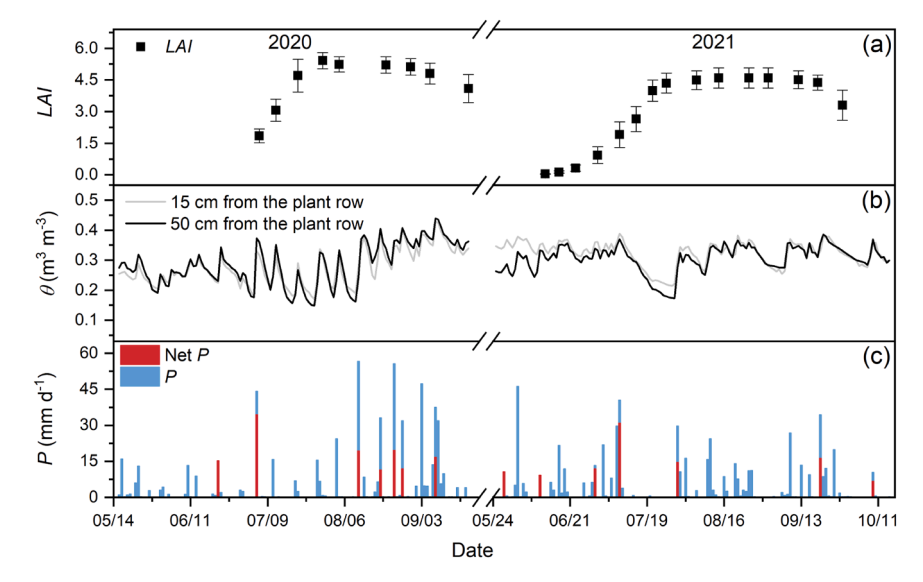


Fig. 2. Dynamics of (a) leaf area index (*LAI*) with standard error bars, (b) daily soil water content (θ) at a depth of 2.5 cm, and (c) the daily precipitation (P) and the net P calculated from Eq. (11).

reached, the average fraction of net *P* reduced to 35% during the silking stage, and increased again to 52% during the maturing stage. The varying patterns of net *P* during the growing season were similar to those of Liu et al. (2015) and Zheng et al. (2018), who claimed that maize leaves could collect and store large amount of rainwater when *LAI* reached the maximum value.

Near-surface θ fluctuated in response to rainfall events and rainfall redistribution below the maize canopy. In 2020, θ values stayed at a relatively low level (0.26 m³ m⁻³ on average) during the seedling stage due to the lack of precipitation events. Several evident wetting-drying cycles appeared in the jointing stage, with an average θ value of 0.24 m³ m⁻³ due to the inadequate rainfall and the increasing water

uptake by the maize plants. Thereafter, the average θ increased to 0.30 m³ m⁻³ (silking stage) and to 0.37 m³ m⁻³ (maturing stage) because of ample precipitation. The θ dynamics in 2021 differed from those in 2020 due to distinct precipitation patterns. During the seedling stage of 2021, θ was generally high (0.32 m³ m⁻³ on average) due to ample rainfalls. The average θ decreased to 0.29 m³ m⁻³ during the jointing stage despite that the largest total amount of rainfall occurred, probably because of a 20-day drying period in July with θ reduction from 0.38 to 0.19 m³ m⁻³. Large θ (0.32 m³ m⁻³ on average) appeared during the silking and maturing stages of 2021 due to the adequate rainfall. The rainfall distribution of P during the growing stages of two years led to a distinct influence on θ . Even with less P, soil water

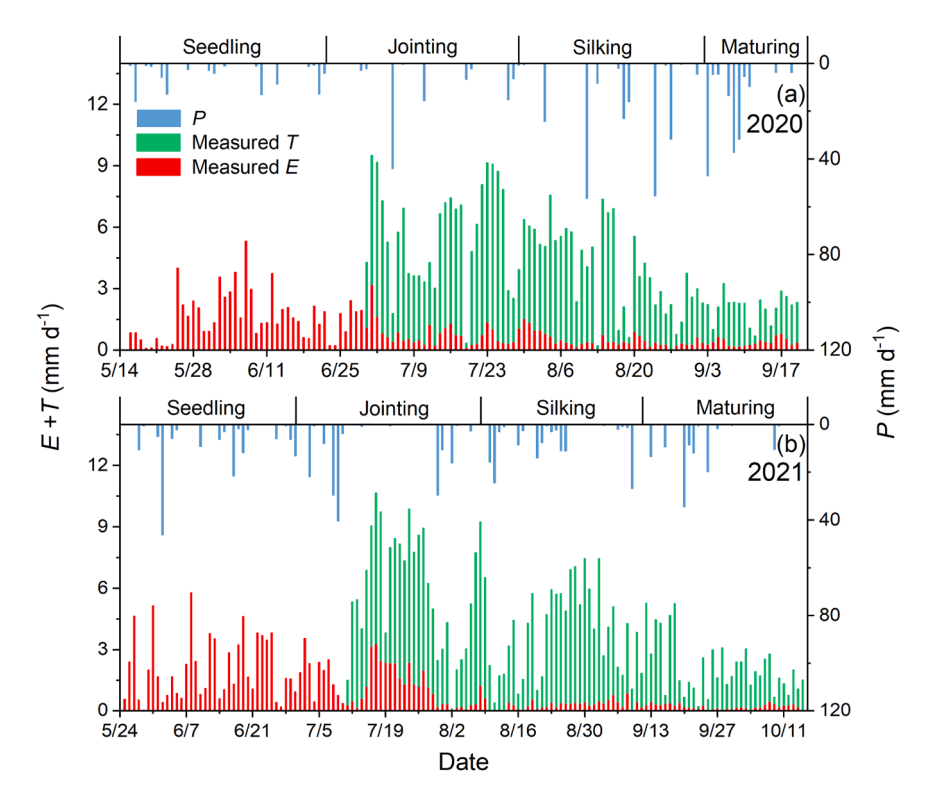


Fig. 3. Daily precipitation amount (*P*, blue bars) and the dynamics of measured daily evaporation (*E*, red bars) and transpiration (*T*, green bars) rates during crop growing seasons in (a) 2020 and (b) 2021.

availability for maize in 2021 was better than that in 2020. Taking the θ of 80% field water capacity (about 0.27 m³ m⁻³) as the critical value for best crop growth, only 66 days within the growing season of 2020 had larger θ values than the critical value, which was fewer than days in 2021 (127 days).

4.3. Dynamics of measured E+T values for the maize field

During the study periods, the dynamics of E and T were measured with heat pulse sensors and sap flow gauges, respectively. In both years, only E was recorded during the seedling stages with a relatively low value (1.9 mm d⁻¹), while large daily E+T values were observed during the jointing (5.0 mm d⁻¹ on average) and silking stages (4.0 mm d⁻¹ on average). Finally, E+T values were reduced to an average value of 2.1 mm d⁻¹ during the maturing stages (Fig. 3).

Fig. 3 and Table 2 show the dynamics of E and T rates, as well as the cumulative values in each growing stage with the development of maize. The cumulative E values in the growing seasons were 121 mm (2020) and 146 mm (2021). Over 52% of the cumulative E, with values of 64 mm (2020) and 76 mm (2021) occurred in the seedling stages. For both growing seasons, the large E during the seedling stage accounted for about 16% of the seasonal ET. In the jointing stages, the cumulative E values were 33 mm (2020) and 51 mm (2021), accounting for 27% and 34% of the total E values. In the silking and maturing stages, E was generally small with cumulative values of 24 mm (2020) and 19 mm (2021), respectively. Daily E rates depicted similar seasonal patterns in 2020 and 2021. For the two growing seasons, a relatively large mean value (1.9 mm d⁻¹) was recorded in the seedling stages, but it decreased to a value of 1.1 mm d⁻¹ in the jointing stages, and finally remained at a small value of 0.4 mm d⁻¹ during the silking and maturing stages.

The seasonal patterns of E rates are driven by meteorological conditions, soil, and plant factors. During the seedling stage, the high WS and low RH enhanced water vapor transfer from the soil to the atmosphere, leading to relatively high E rates (van Bavel and Hillel, 1976). Starting at the jointing stage, canopy shading showed significant influences on E. Rapid LAI increases led to less available energy for latent heat transfer below the canopy, resulting in a sharp decline in E rates (Horton, 1989). During the silking and maturing stages, when the maize canopy fully covered the soil surface (i.e., with the largest LAI values), Erates remained small. In addition, θ also influenced E rates. Compared to 2020, the growing season of 2021 encountered better water condition as indicated by the longer periods with θ greater than 80% field water capacity, which might ensure water supply for surface evaporation. This might explain the larger cumulative E values recorded in 2021 (146 mm) than those in 2020 (121 mm), especially during seedling and jointing stages.

In terms of maize transpiration patterns, it should be noted that T rate measurement was initiated in the jointing stages due to a lack of available sensors for young plants in the seedling stage. In addition, T

measurement in 2020 was terminated during the mid-maturing stage because of instrument failure. Thus, T measurements lasted for 83 and 97 days in 2020 and 2021, respectively. The observed total T values in 2020 and 2021 were 300 mm and 334 mm, respectively, and more than 80% of T occurred during the jointing (147 mm) and silking (123 mm) stages, while only small fractions of T were observed during the maturing stages (10% for 2020 and 19% for 2021 due to different measurement durations) (Table 2). Similar patterns in daily T rates were obtained in both growing seasons. The daily T values averaged 5.0 mm d $^{-1}$ in the jointing stages, decreased to a mean value of 3.5 mm d $^{-1}$ in the silking stages, and finally to a value of 1.8 mm d $^{-1}$ in the maturing stages.

The seasonal and daily variations in T rates were influenced by LAI and R_s . LAI determines the surface area for transpiration, while R_s represents the available energy modulating crop stomatal conductance (Jarvis, 1976; Gan and Liu, 2020). We observed a sharp increase in LAI from 0.9 to 4.5 and a high-level R_s (21 MJ m $^{-2}$ d $^{-1}$ on average) in the jointing stage, which led to the high T rates during this period. Thereafter, although large LAI values were maintained, a slight decline in T rates occurred during the silking stages, possibly caused by the reduction of R_s (17 MJ m $^{-2}$ d $^{-1}$). The lowest T rates were observed in the maturing stages because of the reductions in both LAI and R_s . It is also notable that T depicted sharp decline during the rainfall events due to the low R_s values and reduced vapor pressure deficit on rainy days (Agam et al., 2012). However, following precipitation, daily T values usually increased again due to abundant available soil water for roots (Yunusa et al., 2004).

Generally, the dynamics of E+T in the maize field revealed an E predominance during the seedling stage, followed by T dominance in later stages, which were driven by the interaction of various factors including meteorological conditions (R_s , T_a , WS, RH, P), crop growth (e. g., LAI), and soil water conditions (θ) in each stage.

4.4. Comparisons of net soil water fluxes and measured E+T

Fig. 4 presents temporal variations of measured E+T values, the estimated f, and the daily P. The daily f ranged from -30.0-8.4 mm d⁻¹ in 2020 and -20.3-13.0 mm d⁻¹ in 2021. The positive and negative f values indicated that both upward and downward water fluxes occurred in the near-surface soil layer. In response to rainfall events, downward f fluctuated and lasted for at least 2–3 days depending on the P values. For the periods with continuous rainfall events (lasting for more than 3 days), the downward f could continue for up to 5 days (i.e. June 10–14 in 2020, June 1–5, July 30-August 3, August 10–14, and September 20–24 in 2021). In 2020 and 2021, the largest downward f occurred on July 5 and 9, both following a large rainfall event (P > 40 mm d⁻¹). For the days with or just following the rainfall events, the physical connection between f and ET was lost because both I and E occurred concurrently, thus the ET values differed from f, and Eq. (3) failed.

Table 2 The cumulative and daily values of evaporation (*E*) and transpiration (*T*) during the growing stages in 2020 and 2021.

	Year		Seedling	Jointing	Silking	Maturing	Growing season
Cumulative value (mm)	2020*	E T*	64 -	33 147	17 123	7 30	121 300
	2021	E T	76 -	51 147	11 122	8 65	146 334
Average rate (mm d ⁻¹)	2020	E T	1.7 -	0.9 4.9	0.5 3.5	0.4 1.7	0.9 3.6
	2021	E T	2.1	1.3 5.1	0.3 3.6	0.2 1.9	1.0 3.4

^{*} Note that the use of sap flow gauges required the sprout of maize stem so that the *T* observations started in the jointing stage for both years. The observation period in 2020 was 16 days shorter than that in 2021 due to the early termination of *T* measurements in 2020.

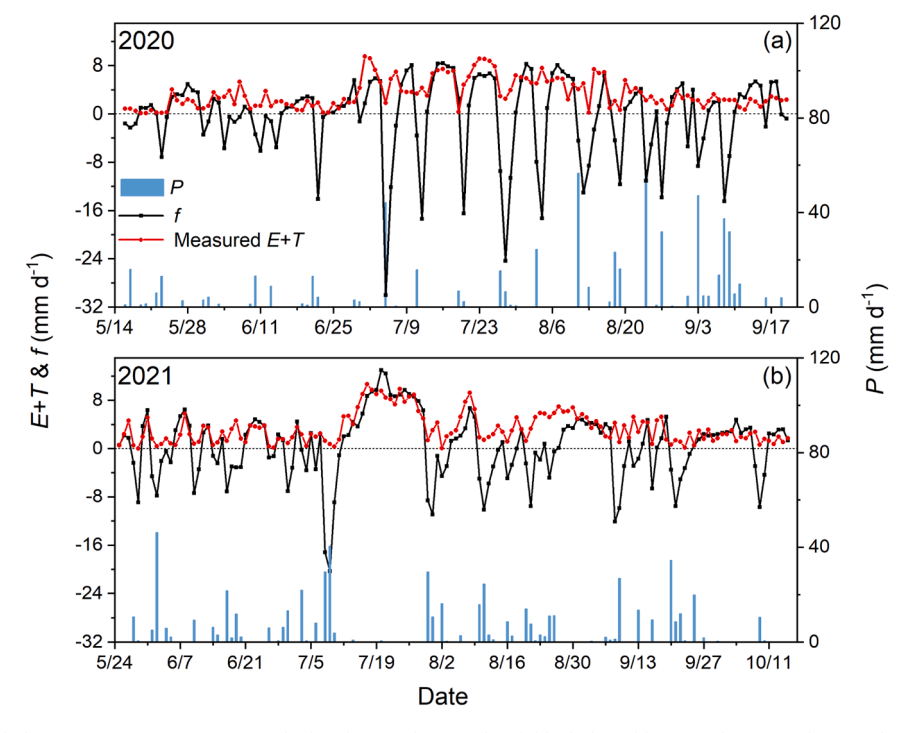


Fig. 4. Temporal values of daily precipitation amount (P), calculated net soil water flux f (black dotted line), and measured E+T values (red dotted line) during the crop growing seasons of (a) 2020 and (b) 2021. The dashed line represents zero f.

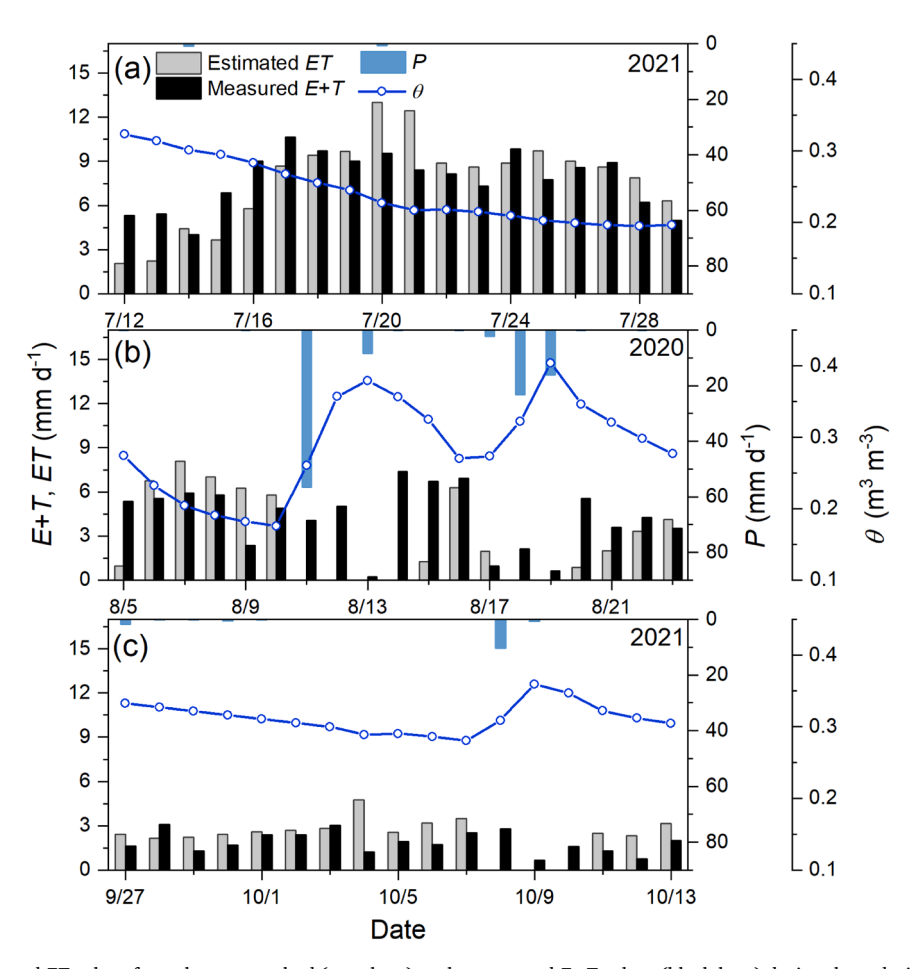


Fig. 5. Comparison of estimated ET values from the new method (gray bars) to the measured E+T values (black bars) during three drying periods with (a) high, (b) medium, and (c) low levels of ET values. The daily precipitation (P) and soil water content (θ) at a depth of 2.5 cm were also included.

The upward f (in positive values) fluctuated and followed the general trend of the measured E+T values during the drying periods (Fig. 4). In the drying period with no downward fluxes in the surface soil layer, ET can be estimated from f using Eq. (3). Similar seasonal variations between the measured E+T values and upward f values were depicted. Upward f values were low during the seedling stages (2.7 mm d $^{-1}$ on average), increased to a mean value of 5.5 mm d $^{-1}$ in the jointing stages, decreased gradually to 3.8 mm d $^{-1}$, and finally to 2.8 mm d $^{-1}$ during the silking and maturing stages.

In general, the upward f and measured E+T values displayed similar temporal trends and daily values, indicating that the new method could provide reliable data. In the early growing stage, however, the measured E+T was lower than the upward f, which was probably caused by the missing T measurements in the seedling stages.

4.5. Comparisons of measured E+T values and estimated ET values

Fig. 5 compares the daily values of the measured E+T to estimated ET(upward f) values during drying periods in the jointing (July 12-29, 2021), silking (August 5-23, 2020) and maturing stages (September 27 to October 13, 2021), representing the cases of high (7.8 mm d^{-1} on average), medium (4.3 mm d⁻¹ on average) and low (1.9 mm d⁻¹ on average) E+T rates, respectively. In general, the estimated daily ETvalues followed the trends of the measured E+T values, except for days when substantial downward fluxes occurred at the 2.5-cm depth during or right after rainfall events (July 12-13 and October 8-10 of 2021, August 5, 11-15 and August 18-21 of 2020). For example, in 2021, the cumulative rainfall of 74 mm during the July 8-9 period resulted in consecutive large downward f values of 17.1 mm d^{-1} and 20.3 mm d^{-1} , and a rapid increase of θ to 0.34 m³ m⁻³ (Fig. 2b). Subsequently the downward f values gradually decreased, and the upward f occurred after July 12. Yet on July 12-13, the ET rates from the new model were underestimated because of the downward fluxes in the near-surface soil layer. After July 14, this effect diminished so that the estimated and measured ET values matched well with an average relative error of 6% in the θ range of 0.30–0.20 m³ m⁻³.

The performance of the new method followed a similar pattern in the medium and low E+T levels. It underestimated ET during periods with increasing or fast declining of θ such as August 11–15 and 18–21 in 2020, October 8–10 in 2021 (Figs. 5b and 5c). This is because I and downward fluxes usually occur during and rightly after rainfall events and diminish during the drying periods. When the days with apparent downward fluxes were excluded, the new method well captured the trends of E+T with RMSEs of 2.02 mm d⁻¹, 1.71 mm d⁻¹, and 1.32 mm d⁻¹ for the high, medium, and low E+T scenarios, respectively.

To quantitively evaluate the performance of the new method, a 1:1 comparison was made between the E+T values from the independent measurements and the estimated ET values from the new method on rain-free days (Fig. 6). The rain-free days were selected if P < 0.6 mm d⁻¹, so that the data for 66 and 77 days in the crop growing seasons of 2020 and 2021 were shown. The data points displayed randomly along the 1:1 line. The correlation analysis gave a slope of 0.94, a coefficient of determination (R²) of 0.85, and a RMSE of 1.93 mm d⁻¹ for the measured and estimated ET values in a range of 0.01–10.6 mm d⁻¹. Although the overall model performance was relatively good, a few scattered data points indicated that the new approach to estimate ET was occasionally prone to large errors due to the occurrence of downward fluxes in the surface soil layer following rainfall events even with positive f.

Previous studies showed the comparisons between ET estimated from the dual K_c and Shuttleworth-Wallace methods and the ET measured from eddy covariance and partitioning method in a vineyard lying in Northwest China led to the R^2 of 0.79 and 0.81 from correlation analysis (Zhao et al., 2015). Jiang et al. (2019) compared the ET values observed from the eddy covariance system with those estimated from the dual K_c method in the arid region of China, and obtained the R^2 and

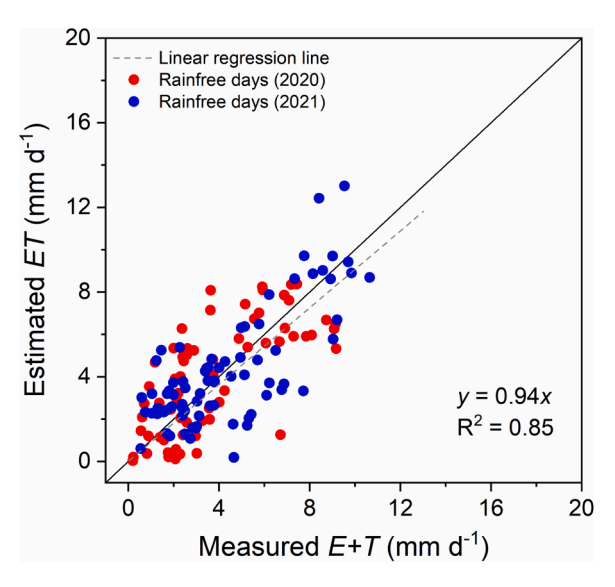


Fig. 6. A 1:1 comparison between measured E+T values and estimated ET values on rain-free days during the maize growing seasons in 2020 (red dots) and 2021 (blue dots). The grey dashed line represents the linear regression line.

RMSE in the range of (0.60-0.76) and $(0.80-1.05 \text{ mm d}^{-1})$ for the ET range of $0-8 \text{ mm d}^{-1}$. Our study also gave a similar R^2 value in ET estimations, but relatively larger RMSE values than the literature values due to the large absolute value of ET at the local site in the semi-humid region of Northeast China. Overall, our new method performs well on rain-free days during the two crop growing seasons, indicating that it is a reliable and efficient way to make ET estimations in a rainfed maize field with paired-row planting patterns.

The performance of the new model is affected by several factors. First, errors in the estimated ET can come from the assumption of onedimensional water flow in near-surface soils. In a row-cropped field, lateral water flow across the row might arise due to root water uptake, or thermally driven water transfer under certain circumstances (Kool et al., 2014; Lu et al., 2020). Additionally, the uncertainties in D values can lead to biased ET estimates. The calibrated D values in the sub-periods, within the range of 92–2331 cm² d⁻¹, are listed in Table A1. The results were consistent with the values from previous studies on clay loam soils, e.g., the fitted D value of 987 cm² d⁻¹ from the simulation study of Sadeghi et al. (2019), and the laboratory-measured D values in the range of 100–2000 cm² d⁻¹ (at θ from 0.1 to 0.4 m³ m⁻³) obtained by Zheng et al. (2014) and Gao et al. (2019). However, it should be noted that D is also related to soil structure and bulk density which is influenced by soil tillage and wetting-drying cycles (Baruah and Hasegawa, 2001; He et al., 2010). Therefore, further study should address the changes of D as related to the spatial and temporal variations of soil bulk density and structure during crop growing season (Sadeghi et al., 2022).

It should be noted that Black et al. (1969) presented a simple model in diffusion form based on the analytical solution to Richards' equation to estimate *E*. Similar work can be found in Sadeghi et al. (2022), and they proposed an approximate solution to the linearized Richards' equation that accounts for both gravitation and diffusion processes. These implies a further research demand to use the simplified solution for field *ET* estimations.

5. Conclusion

This study presents a new method to estimate daily ET rates in a rainfed maize field in Northeast China. The approach was evaluated using independent measurements of E and T values with heat pulse sensors and sap flow gauges during two growing seasons. Under a paired-row planting pattern, E accounted for about 16% of the total ET

in the growing seasons, with a predominance of E in the seedling stage. With fully-developed canopy cover, E sharply decreased to a value of 0.4 mm d $^{-1}$, and T accounted for \sim 89% of ET since the silking stage. For the new model performance, on rain-free days, ET estimated from the new method closely agreed with measured values, with a R 2 of 0.85 for both years. On rainy periods or a few days following large rainfall events, the new method failed to give reasonable ET estimates because of the existence of downward F. Overall, the new method provides an alternative way to quantify FT based on soil water content, FT and rainfall information.

CRediT authorship contribution statement

Yutong Liu: Writing – original draft, Methodology, Formal analysis, Data curation. Robert Horton: Writing – review & editing, Validation, Funding acquisition. Tusheng Ren: Writing – review & editing, Supervision, Resources, Funding acquisition. Yili Lu: Writing – review & editing, Supervision, Funding acquisition. Morteza Sadeghi: Writing – review & editing, Methodology, Formal analysis.

Declaration of Competing Interest

The authors declare the following financial interests/personal

relationships which may be considered as potential competing interests: Tusheng Ren reports article publishing charges was provided by the Strategic Priority Research Program of the Chinese Academy of Sciences. Yili Lu reports statistical analysis and travel were provided by National Natural Science Foundation of China. Robert Horton reports writing assistance was provided by U.S. National Science Foundation. Robert Horton reports statistical analysis and writing assistance were provided by USDA-NIFA Multi-State Project. If there are other authors, they declare that they have no known competing financial interests or personal relationships that could have appeared to influence the work reported in this paper.

Data Availability

Data will be made available on request.

Acknowledgments

This work is supported by the Strategic Priority Research Program of the Chinese Academy of Sciences (Grant No. XDA28010402), the National Natural Science Foundation of China (Grant No. 42307390), U.S. National Science Foundation under Grant 2037504, and USDA-NIFA Multi-State Project 4188.

Appendix A

For the calibration of soil water diffusivity (D), the plant growing season was divided into (n + 1) time intervals based on the number (n) of large rainfall events (i.e. $P > 30 \text{ mm d}^{-1}$), denoted by S_1 , S_2 , ..., S_n , S_{n+1} , and marked with 'large rainfall' events of P_1 , P_2 , ..., P_{n-1} , P_n . Here S_1 extends from DOY(initial) to DOY(P_1), S_2 from DOY(P_1) to DOY(P_2), ..., S_n from DOY(P_{n-1}) to DOY(P_n), and S_{n+1} from DOY(P_n) to DOY(end). In this study, maize growing seasons in 2020 and 2021 were divided into 5 sub-periods, respectively. The D values as well as the initial and the actual maximum net soil water flux (f_{max} and f_{max}) based on calibration procedures were shown in Table A1.

Table A1

The sub-periods, the soil water diffusivity (D), the actual maximum net soil water flux (fmax), and the initial maximum net soil water flux (fmax) calculated from the calibration procedures were listed. Locations 1 and 2 represent the two replicates of in-row soil water content measurements.

Year	Location	Sub-periods	$f_{\rm max}$ (cm d ⁻¹)	$f_{ m max}$ (cm d ⁻¹)	D (cm ² d ⁻¹)
2020	1	5/16–7/4	1.1	1.5	183
		7/5-8/10	2.0	3.4	304
		8/11-8/23	1.4	1.9	196
		8/24-9/2	0.6	2.0	1023
		9/3-9/20	0.7	1.7	494
	2	5/16-7/4	1.1	1.5	195
		7/5-8/10	1.4	3.4	565
		8/11-8/23	1.2	1.1	84
		8/24-9/2	0.8	1.2	199
		9/3-9/20	0.8	1.7	410
2021	1	5/25-6/1	0.2	1.1	2331
		6/2-7/7	0.7	0.9	182
		7/8-7/29	0.8	3.1	1330
		7/30-9/19	0.8	1.5	322
		9/20-10/15	0.7	0.7	92
	2	5/25-6/1	0.3	1.1	1526
		6/2-7/7	0.4	1.2	1131
		7/8-7/29	0.8	3.1	1403
		7/30-9/19	0.7	1.5	440
		9/20–10/15	0.6	1.6	821

References

Agam, N., Evett, S.R., Tolk, J.A., Kustas, W.P., Colaizzi, P.D., Alfieri, J.G., McKee, L.G., Copeland, K.S., Howell, T.A., Chávez, J.L., 2012. Evaporative loss from irrigated interrows in a highly advective semi-arid agricultural area. Adv. Water Resour. 50, 20–30. Akbar, R., Gianotti, D.S., McColl, K.A., Haghighi, E., Salvucci, G.D., Entekhabi, D., 2018. Hydrological storage length scales represented by remote sensing estimates of soil moisture and precipitation. Water Resour. Res. 54, 1476–1492.

Allen, R.G., Pereira, L.S., Raes, D., Smith, M., 1998. Crop evapotranspiration: guidelines for computing crop water requirements. In: United Nations FAO, Irrigation and Drainage Paper 56. FAO, Rome, Italy.

Allen, R.G., Pereira, L.S., Howell, T.A., Jensen, M.E., 2011. Evapotranspiration information reporting: I. Factors governing measurement accuracy. Agric. Water Manag. 98, 899–920.

- Baldocchi, D., Falge, E., Gu, L.H., Olson, R., Hollinger, D., Running, S., Anthoni, P., Bernhofer, C., Davis, K., Evans, R., Fuentes, J., Goldstein, A., Katul, G., Law, B., Lee, X.H., Malhi, Y., Meyers, T., Munger, W., Oechel, W., K.T.P, U., Pilegaard, K., Schmid, H.P., Valentini, R., Verma, S., Vesala, T., Wilson, K., Wofsy, S., 2001. FLUXNET: A new tool to study the temporal and spatial variability of ecosystem-scale carbon dioxide, water vapor, and energy flux densities. Bull. Am. Meteorol. Soc. 82, 2415–2434.
- Baruah, T.C., Hasegawa, S., 2001. In-situ measurement of soil evaporation from a volcanic ash soil by TDR technique using soil water diffusivity. Geoderma 102, 317–328.
- van Bavel, C.H.M., Hillel, D.I., 1976. Calculating potential and actual evaporation from a bare soil surface by simulation of concurrent flow of water and heat. Agric. . Meteorol. 17, 453–476.
- Black, T.A., Gardner, W.R., Thurtell, G.W., 1969. Prediction of evaporation, drainage, and soil water storage for a bare soil. Soil Sci. Soc. Am. J. 33, 655–661.
- Cammalleri, C., Anderson, M.C., Gao, F., Hain, C.R., Kustas, W.P., 2013. A data fusion approach for mapping daily evapotranspiration at field scale. Water Resour. Res. 49, 4672–4686.
- Cholpankulov, E.D., Inchenkova, O.P., Paredes, P., Pereira, L.S., 2008. Cotton irrigation scheduling in central Asia: Model calibration and validation with consideration of groundwater contribution. Irrig. Drain. 57, 516–532.
- Coopersmith, E.J., Bell, J.E., Cosh, M.H., 2015. Extending the soil moisture data record of the U.S. Climate Reference Network (USCRN) and Soil Climate Analysis Network (SCAN). Adv. Water Resour. 79, 80–90.
- Evett, S.R., Schwartz, R.C., Casanova, J.J., Heng, L.K., 2012. Soil water sensing for water balance, ET and WUE. Agric. Water Manag. 104, 1–9.
- Famiglietti, J.S., Devereaux, J.A., Laymon, C.A., Tsegaye, T., Houser, P.R., Jackson, T.J., Graham, S.T., Rodell, M., van Oevelen, P.J., 1999. Ground-based investigation of soil moisture variability within remote sensing footprints during the Southern Great Plains 1997 (SGP97) Hydrology Experiment. Water Resour. Res. 35, 1839–1851.
- Forsythe, W.E., 1964. Smithsonian physical tables. Smithsonian Institution Publication 4169, Washington, DC.
- Fuchs, M., Tanner, C.B., 1970. Error analysis of Bowen ratios measured by differential psychrometry. Agric. Meteorol. 7, 329–334.
- Gan, G., Liu, Y., 2020. Inferring transpiration from evapotranspiration: A transpiration indicator using the Priestley-Taylor coefficient of wet environment. Ecol. Indic. 110, 105853.
- Gao, Y.X., Liu, J.C., Feng, X., Zhang, Y.P., Zhang, B., 2019. Experimental study on unsaturated soil water diffusivity in different soils in Hebei. Piedmont Plain. J. Groundw. Sci. Eng. 7, 165–172.
- He, J., Li, H., Kuhn, N.J., Wang, Q., Zhang, X., 2010. Effect of ridge tillage, no-tillage, and conventional tillage on soil temperature, water use, and crop performance in cold and semi-arid areas in Northeast China. Aust. J. Soil Res 48, 737–744.
- Heitman, J.L., Horton, R., Sauer, T.J., DeSutter, T.M., 2008. Sensible heat observations reveal soil-water evaporation dynamics. J. Hydrometeorol. 9, 165–171.
- Holmes, J.W., 1984. Measuring evapotranspiration by hydrological methods. Agric. Water Manag. 8, 29–40.
- Horton, R., 1989. Canopy shading effects on soil heat and water flow. Soil Sci. Soc. Am. J. 53, 669–679.
- Hupet, F., Vanclooster, M., 2005. Micro-variability of hydrological processes at the maize row scale: implications for soil water content measurements and evapotranspiration estimates. J. Hydrol. 303, 247–270.
- Jarvis, P.G., 1976. Interpretation of variations in leaf water potential and stomatal conductance found in canopies in field. Philos. Trans. R. Soc. Lond. B. 273, 593–610.
- Jiang, X.L., Kang, S.Z., Tong, L., Li, S.E., Ding, R.S., Du, T.S., 2019. Modeling evapotranspiration and its components of maize for seed production in an arid region of northwest China using a dual crop coefficient and multisource models. Agric. Water Manag. 222, 105–117.
- Kool, D., Ben-Gal, A., Agam, N., Šimůnek, J., Heitman, J.L., Sauer, T.J., Lazarovitch, N., 2014. Spatial and diurnal below canopy evaporation in a desert vineyard: Measurements and modeling. Water Resour. Res. 50, 7035–7049.
- Koster, R.D., Crow, W.T., Reichle, R.H., Mahanama, S.P., 2018. Estimating basin-scale water budgets with SMAP soil moisture data. Water Resour. Res. 54, 4228–4244.
- Liu, H., Zhang, R., Zhang, L., Wang, X., Li, Y., Huang, G., 2015. Stemflow of water on maize and its influencing factors. Agric. Water Manag. 158, 35–41.
- Liu, Y., Pereira, L.S., Fernando, R.M., 2006. Fluxes through the bottom boundary of the root zone in silty soils: Parametric approaches to estimate groundwater contribution and percolation. Agric. Water Manag. 84, 27–40.
- Lu, J., Zhang, Q., Werner, A.D., Li, Y., Jiang, S., Tan, Z., 2020. Root-induced changes of soil hydraulic properties - A review. J. Hydrol. 589, 125203.
- Lu, Y., Dong, J., Steele-Dunne, S.C., van de Giesen, N., 2016. Estimating surface turbulent heat fluxes from land surface temperature and soil moisture observations using the particle batch smoother. Water Resour. Res. 52, 9086–9108.

- Luo, C., Wang, Z., Sauer, T.J., Helmers, M.J., Horton, R., 2018. Portable canopy chamber measurements of evapotranspiration in corn, soybean, and reconstructed prairie. Agric. Water Manag. 198, 1–9.
- Metzger, J.C., Wutzler, T., Dalla Valle, N., Filipzik, J., Grauer, C., Lehmann, R., Roggenbuck, M., Schelhorn, D., Weckmüller, J., Küsel, K., Totsche, K.U., Trumbore, S., Hildebrandt, A., 2017. Vegetation impacts soil water content patterns by shaping canopy water fluxes and soil properties. Hydrol. Process. 31, 3783–3795.
- Monteith, J.L., 1965. Evaporation and the environment. Symp. Soc. Exp. Biol. 19, 205–234.
- Ochsner, T.E., Sauer, T.J., Horton, R., 2007. Soil heat storage measurements in energy balance studies. Agron. J. 99, 311–319.
- Penman, H.L., 1948. Natural evaporation from open water, bare soil and grass. Proc. R. Soc. Lond. A. 193, 120–145.
- Pereira, L.S., Allen, R.G., Smith, M., Raes, D., 2015. Crop evapotranspiration estimation with FAO56: Past and future. Agric. Water Manag. 147, 4–20.
- Purdy, A.J., Fisher, J.B., Goulden, M.L., Colliander, A., Halverson, G., Tu, K., Farniglietti, J.S., 2018. SMAP soil moisture improves global evapotranspiration. Remote Sens. Environ. 219, 1–14.
- Rana, G., Katerji, N., 2000. Measurement and estimation of actual evapotranspiration in the field under Mediterranean climate: A review. Eur. J. Agron. 13, 125–153.
- Sadeghi, M., Tuller, M., Warrick, A.W., Babaeian, E., Parajuli, K., Gohardoust, M.R., Jones, S.B., 2019. An analytical model for estimation of land surface net water flux from near-surface soil moisture observations. J. Hydrol. 570, 26–37.
- Sadeghi, M., Hatch, T., Huang, G., Bandara, U., Ghorbani, A., Dogrul, E.C., 2022.
 Estimating soil water flux from single-depth soil moisture data. J. Hydrol. 610, 127999
- Schmugge, T.J., Kustas, W.P., Ritchie, J.C., Jackson, T.J., Rango, A., 2002. Remote sensing in hydrology. Adv. Water Resour. 25, 1367–1385.
- Sharratt, B.S., 1993. Water use, intercepted radiation, and soil temperature of skip-row and equidistant-row barley. Agron. J. 85, 686–691.
- Wang, Y., Zhang, X., Xiao, X., Heitman, J., Horton, R., Ren, T., 2017. An empirical calibration for heat-balance sap-flow sensors in maize. Agron. J. 109, 1122–1128.
- Wang, Y., Horton, R., Xue, X., Ren, T., 2021. Partitioning evapotranspiration by measuring soil water evaporation with heat-pulse sensors and plant transpiration with sap flow gauges. Agric. Water Manag. 252, 106883.
- Wang, Z., Luo, C., Sauer, T., Helmers, M.J., Xu, L., Horton, R., 2018. Canopy chamber measurements of carbon dioxide fluxes in corn and soybean fields. Vadose Zone J. 17. 1–5.
- Wang, Z., Timlin, D., Kouznetsov, M., Fleisher, D., Li, S., Tully, K., Reddy, V., 2020.
 Coupled model of surface runoff and surface-subsurface water movement. Adv.
 Water Resour. 137, 103499.
- Warrick, A.W., 1975. Analytical solutions to one-dimensional linearized moisture flow equation for arbitrary input. Soil Sci. 120, 79–84.
- Xiao, X., Heitman, J.L., Sauer, T.J., Ren, T., Horton, R., 2014. Sensible heat balance measurements of soil water evaporation beneath a maize canopy. Soil Sci. Soc. Am. J. 78, 361–368.
- Xiao, X., Sauer, T.J., Singer, J.W., Horton, T., Ren, J.L., 2016. Partitioning evaporation and transpiration in a maize field using heat-pulse sensors for evaporation measurement. Trans. Asabe 59, 591–599.
- Yunusa, I.A.M., Walker, R.R., Lu, P., 2004. Evapotranspiration components from energy balance, sapflow and microlysimetry techniques for an irrigated vineyard in inland Australia. Agric. . Meteorol. 127, 93–107.
- Zhang, R., Seki, K., Wang, L., 2023. Quantifying the contribution of meteorological factors and plant traits to canopy interception under maize cropland. Agric. Water Manag. 279, 108195.
- Zhang, X., Heitman, J., Horton, R., Ren, T., 2014. Measuring near-surface soil thermal properties with the heat-pulse method: correction of ambient temperature and soilair interface effects. Soil Sci. Soc. Am. J. 78, 1575–1583.
- Zhao, P., Li, S., Li, F., Du, T., Tong, L., Kang, S., 2015. Comparison of dual crop coefficient method and Shuttleworth-Wallace model in evapotranspiration partitioning in a vineyard of northwest China. Agric. Water Manag. 160, 41–56.
- Zheng, J., Wang, Y., Ren, Q.H., Wan, J.X., 2014. Impacts of maize straw additive on soil water evaporation with sandy loam in the region of Jingtai, Gansu province. Adv. Mat. Res. 864-867, 2606–2613.
- Zheng, J., Fan, J., Zhang, F., Yan, S., Xiang, Y., 2018. Rainfall partitioning into throughfall, stemflow and interception loss by maize canopy on the semi-arid Loess Plateau of China. Agric. Water Manag. 195, 25–36.
- Zreda, M., Desilets, D., Ferre, T.P.A., Scott, R.L., 2008. Measuring soil moisture content non-invasively at intermediate spatial scale using cosmic-ray neutrons. Geophys. Res. Lett. 35, 402–407.